INORGANIC CHEMISTRY FRONTIERS

RESEARCH ARTICLE

View Article Online
View Journal | View Issue

Cite this: *Inorg. Chem. Front.*, 2022, **9**, 3282

A POM-based porous supramolecular framework for efficient sulfide–sulfoxide transformations with a low molar O/S ratio†

Yanhong Chen, Haiyan An, * Shenzhen Chang, Yanqin Li, Qingshan Zhu, Huiyun Luo and Yaohui Huang

The selective oxidation of organic sulfides is a pivotal step in the preparation of sulfoxides that can act as synthetic intermediates when preparing fine chemicals, bioactive molecules, and asymmetric catalysis ligands. To construct high-performance heterogeneous catalysts for sulfide-sulfoxide transformations, herein, we designed and synthesized a supramolecular porous catalyst based on ε-Keggin polyoxometalates (POMs), $TBA_2H_2[Zn_4(im)(Him)_2][\varepsilon\text{-}PMo_8^{V}Mo_4^{VI}O_{40}]\cdot 3H_2O$ (**1**, Him = 1*H*-imidazole). Single-crystal X-ray diffraction analysis indicates that the porous framework of **1** can be obtained *via* the supramolecular stacking of one-dimensional helical chains alternately linked by Zn_4-ε-Keggin clusters and Him ligands. During the selective oxidation of methyl phenyl sulfide to methyl phenyl sulfoxide (MPSO), compound **1** achieved a >99% yield toward MPSO and 90.3% oxidant utilization efficiency within 10 min. The corresponding turnover frequency (TOF), expressing catalytic activity, was up to 1200 h^{-1}. The catalyst also demonstrated extensive substrate tolerance during catalysis, and the corresponding yields of sulfoxides were satisfactory when only 1.2 equivalents of oxidant were used. Besides this, **1** can also effectively degrade a sulfur mustard simulant (2-chloroethyl ethyl sulfide) to the nontoxic product 2-chloroethyl ethyl sulfoxide within 10 min at room temperature, with an oxidant utilization efficiency of up to 94.5%. Importantly, the excellent catalytic activity of compound **1** was also proven *via* comparison with an analogous 3D compound **2** (TOF = 800 h^{-1} at full MPS conversion), $TBAH_2[K(Him)(im)][Zn_4(Him)(Hip)][\varepsilon\text{-}PMo_8^{V}Mo_4^{VI}O_{40}]$ (Hip = 4-(1*H*-imidazol-2-yl)-pyridine), which was covalently assembled from one-dimensional Zn4-ε-Keggin POM chains and metal–organic units. Moreover, the truly heterogeneous nature of **1** and **2** was confirmed *via* cycling and hot-filtration experiments, and their structural stability was verified based on Fourier-transform infrared spectra and powder X-ray diffractometry (PXRD) patterns.

Received 9th March 2022,
Accepted 20th May 2022

DOI: 10.1039/d2qi00525e

rsc.li/frontiers-inorganic

1. Introduction

Sulfide–sulfoxide selective transformation represents one of the most important and fascinating reactions from both chemical and biological perspectives, which has long been used in synthesizing high-value sulfoxide intermediates with biological activity and purifying toxic and harmful sulfur-containing chemicals such as sulfur-containing chemical weapons or fuels.[1–8] Currently, the large-scale oxidation of sulfides remains prevalent, with unfashionable 'stoichiometric' technologies including hypervalent metal- or iodine-containing oxidants (Cr^{6+}, MnO_2, MnO_4^-, IO_3^-, *etc.*) and strong mineral acids (H_2SO_4, HNO_3, H_3PO_4).[9] Therefore, the design and development of environmentally-friendly catalytic technologies for the selective oxidation of sulfides using green oxidants such as molecular oxygen, aqueous hydrogen peroxide, or organic peroxide are desired to overcome the shortcomings of conventional procedures.[10–13]

Polyoxometalates (POMs), as a subset of crystalline metal oxide catalysts with compatibility with various oxygen sources, good redox properties, tunable acidities and alkalinities, and good solubility stability, have broadly been proven to be effective and green in catalyzing the selective oxidation of organic substances.[14–18] Among them, many POM-based catalytic systems for oxidizing sulfides have been successfully

State Key Laboratory of Fine Chemicals, School of Chemical Engineering, Dalian University of Technology, Dalian 116023, People's Republic of China.
E-mail: anhy@dlut.edu.cn; Fax: +86-411-84657675; Tel: +86-411-84657675

†Electronic supplementary information (ESI) available: Characterization details, synthetic procedures, supplementary structure diagrams, supplementary catalytic results, and the calculation of oxidant utilization efficiency. CCDC 2120945 and 2120946. For ESI and crystallographic data in CIF or other electronic format see DOI: **https://doi.org/10.1039/d2qi00525e**

established over the past dozen years.[19–21] Examples that have easily come to conception are the selective oxidation of a variety of thioethers and degradation of sulfur mustard gas simulants (2-chloroethyl ethyl sulfide, CEES) catalyzed by inorganic POMs such as $TBA_4[\alpha\text{-}Mo_8O_{26}]$, $TBA_{12}H_{13}PNb_{12}O_{40}(V^{V}O)_2(V_4{}^{IV}O_{12})_2$, $TBA_4H_2[BW_{11}Mn(H_2O)O_{39}]$, and $TBA_8[(\gamma\text{-}SiW_{10}Ti_2O_{38}(OH)_2)_2]$ under homogeneous conditions.[22–25] In recent years, increasingly more research has been gradually focused on the construction of POM-based heterogeneous catalysts. Immobilizing POMs on proper supports (*e.g.*, MOFs, COFs, high surface area carbon, mesoporous silica and metal oxides) has been widely employed to achieve the heterogeneity of POMs.[26–30] However, some shortcomings of the above systems involve their (i) ill-defined structures, (ii) leachable active sites, and (iii) low specific surface area and exposure of active sites, which restrict their practical applications. A feasible scheme of late has been to construct crystalline POM-based metal–organic complexes, which can not only disperse the POM at the molecular level, but also easily clarify its structure–activity relationship.[31] Numerous studies have proven that covalently bonded POM-based metal–organic complexes possess excellent catalytic and recycling properties in the heterogeneous catalytic selective oxidation of sulfide to sulfoxide.[32–37] Nevertheless, most of the covalently bonded skeleton blocks the accessibility of internal sites and mass transfer process, which in turn requires a high oxygen–sulfur ratio to achieve high conversion, and to a certain extent is not conducive to the economy and environmental protection.

Recently, there has been a surge in research interest on POM-based porous supramolecular frameworks with periodic and accessible channels because their non-covalent skeletons have strong reversibility and their porous structures also allow fast mass transfer.[38–42] However, few catalytic systems based on POM-based porous supramolecular frameworks have been exploited until now.[12,42,43] For instance, a porous framework with 27.6% void space constructed *via* the supramolecular stacking of Keggin-type POMs and metalloporphyrin layers has been shown to exhibit high activity towards the conversion of appropriately sized alkylbenzenes to ketones.[44] Zhang *et al.* reported a feasible supramolecular self-assembly route to fabricate a series of POM-based porous frameworks with catalytic activity for dye degradation and esterification.[45] Our group has recently prepared two POM-based porous supramolecular frameworks constituted by Keggin-type POMs and Cu-organic units, which show excellent catalytic activity in the oxidation of substituted phenols to the corresponding *p*-benzoquinones.[12] In terms of the oxidation of sulfides, Hu, *et al.* found that a 3D polyoxovanadate-based supramolecular porous framework as an excellent heterogeneous catalyst can effectively realize the selective oxidation of sulfides and degradation of CEES.[35] Very recently, a 3D Waugh-type POM-based supramolecular porous framework was demonstrated by Wang and co-workers to provide more active sites than its 2D covalently bonded analogs and thus exhibit higher catalytic activity in the oxidation of thioethers.[46] Be that as it may, the rudimentary research status still inspires us to pursue more stable POM-based porous supramolecular frameworks with excellent catalytic performance for the oxidation of sulfides.

In this work, a novel Zn_4-capped ε-Keggin-type POM-based porous framework, $TBA_2H_2[Zn_4(im)(Him)_2][\varepsilon\text{-}PMo_8{}^{V}Mo_4{}^{VI}O_{40}]\cdot 3H_2O$ (**1**, Him = imidazole), formed from one-dimensional helical chains *via* supramolecular interactions (hydrogen bonding) has been designed and synthesized. As expected, compound **1** exhibits excellent performance to selectively oxidize various sulfides to sulfoxides and rapidly detoxify CEES in the presence of aqueous hydroperoxide as a green oxidant under a low oxygen–sulfur ratio (O/S = 1.2). Within 10 min, for the oxidation of methyl phenyl sulfide (MPS), the yield of methyl phenyl sulfoxide (MPSO) was close to 100% with H_2O_2 utilization efficiency >90%. The corresponding catalytic activity expressed by the turnover frequency (TOF) was also as high as 1200 h^{-1}. Additionally, in exploring the synthesis conditions of **1**, we also obtained a new POM-based metal–organic coordination polymer with a 3D covalent framework, $TBAH_2[K(Him)(im)][Zn_4(Him)(Hip)][\varepsilon\text{-}PMo_8{}^{V}Mo_4^{VI}O_{40}]$ (**2**, Hip = 4-(1*H*-imidazol-2-yl)-pyridine), composed of one-dimensional Zn_4-ε-Keggin POM inorganic chains and metal–organic units. Compound **2** also showed excellent catalytic activity in the oxidation of sulfides (for MPS–MPSO transformation the TOF was 800 h^{-1}), but it was still inferior to compound **1**, which further indicated that the supramolecular porous framework of compound **1** was more conducive to mass transfer and featured more exposed internal active sites.

2. Experimental

The details of instruments, detailed operation of the detection of hydrogen peroxide, and X-ray crystallographic studies are provided in Section I of the ESI.†

2.1 Synthesis of $TBA_2H_2[Zn_4(im)(Him)_2][\varepsilon\text{-}PMo_8{}^{V}Mo_4{}^{VI}O_{40}]\cdot 3H_2O$ (1)

A mixture of $(NH_4)_6Mo_7O_{24}\cdot 4H_2O$ (0.30 g, 0.24 mmol), H_3PO_3 (0.03 g, 0.36 mmol), $Zn(Ac)_2\cdot 2H_2O$ (0.11 g, 0.5 mmol), 25 wt% solution of tetrabutylammonium hydroxide in water (200 μL, 0.19 mmol), and H_2O (8 mL) were stirred for 30 min at room temperature, and the pH was adjusted to 5.50 with 2 M HCl. Subsequently, molybdenum powder 99.5% (0.03 g, 0.31 mmol), 2-(pyridinium-4-yl)-1*H*-imidazole-4,5-dicarboxylic acid (0.05 g, 0.21 mmol) and 1*H*-imidazol (0.08 g, 1.18 mmol) were successively added. Then, the suspension was put into a 25 mL Teflon-lined stainless-steel autoclave and kept at 180 °C for 3 days. After cooling slowly to room temperature, the black polyhedral crystals were collected by filtering and washed with distilled water (yield: 52.8% based on $(NH_4)_6Mo_7O_{24}\cdot 4H_2O$). Elemental analysis (%) for $H_{89}C_{41}N_8O_{42}PZn_4Mo_{12}$, calcd: C, 17.52; H, 3.19; N, 3.99. Found: C, 17.36; H, 3.43; N, 4.11. IR (KBr Pellet, cm^{-1}): 3548 (w), 3392 (w), 3131 (w), 2964 (w), 2873 (w), 1618 (w), 1466 (m), 1383 (w), 1327 (w), 1267 (w), 1076 (m), 964 (w), 937 (s), 814 (w), 785 (s), 708 (m), 638 (w), 594 (m).

2.2 Synthesis of $TBAH_2[K(Him)(im)][Zn_4(Him)(Hip)][\varepsilon\text{-}PMo_8{}^{V}Mo_4{}^{VI}O_{40}]$ (2)

Compound **2** was produced by adjusting the pH of the synthesis system of compound **1**, that is, from 5.50 to 5.10. After standing at 180 °C for 3 days, the black strip crystals were obtained, washed with water and dried in air (yield: 45.4% based on Hip). Elemental analysis (%) for $C_{33}H_{56}KMo_{12}N_{10}O_{40}PZn_4$, calcd: C, 14.59; H, 2.08; N, 5.16. Found: C, 14.56; H, 2.13; N, 5.24. IR (KBr Pellet, cm^{-1}): 3440 (w), 3274 (w), 3182 (w), 2960 (w), 2870 (w), 1626 (w), 1545 (w), 1512 (w), 1452 (w), 1410 (w), 1327 (w), 1259 (w), 1174 (w), 1138 (w), 1070 (m), 935 (s), 818 (w), 785 (s), 717 (w), 656 (w), 617 (w), 586 (m).

2.3 Typical process for the oxidation of sulfides

In a typical operation, the substrates (0.25 mmol), the powdered catalysts (1.25 μmol, activated for 12 h under vacuum at 150 °C), the internal standard (naphthalene or octane, 0.25 mmol), and the solvents (MeOH, 0.5 mL) were added successively into a glass reactor (1.5 mL) at room temperature. The mixture was first stirred at 50 °C for a certain period of time, then the oxidant (30% H_2O_2, 0.3 mmol) was added and timing began. The progress of the reaction was monitored by gas chromatography (GC) analysis. The corresponding products were distinguished by GC/MS or ^{1}H NMR (Table S7†). The conversion of the sulfides and the selectivity of sulfoxides were calculated by the internal standard method of GC. The blank experiments in the absence of catalysts, oxidants or both, and other control variable comparison experiments were also carried out in a similar way to the above-mentioned preparation. Cycling experiments were carried out with the model reaction (MPS–MPSO transformation) as the research object. Specifically, the catalysts were firstly separated *via* centrifugation before recycling, then washed with MeOH three times, and dried in air. In multi-cycle continuous experiments, the initial mol of MPS and H_2O_2 were maintained at 0.25 mmol and 0.30 mmol by continuous addition after the reaction in the previous cycle. In a typical experiment of the oxidative degradation of CEES, all the operations were similar to those mentioned above except for adjusting the temperature to room temperature.

3. Results and discussion

3.1 Structural description

X-ray crystallographic data demonstrate that **1** crystallizes in the tetragonal space group $I4_1/a$ with sixteen formula units (Z = 16) per unit cell, while **2** crystallizes in the monoclinic space group $P2_1/n$ with four formula units (Z = 4) per unit cell (Table S1†). The POM building units in **1** and **2** reveal classic ε-Keggin structural characteristics, with four $\{Mo_3O_{13}\}$ moieties capped by four tetrahedral Zn^{II} ions. In **1** and **2**, the valences of the Mo ions were determined through bond valence sum (BVS) calculations and further confirmed by the Mo–Mo distances (Table S2†).[47] More specifically, the BVS calculations of Mo ions are 5.29 (Mo1), 5.33 (Mo2), 5.27 (Mo3), 6.02 (Mo4), 5.22 (Mo5), 5.45 (Mo6), 6.18 (Mo7), 6.06 (Mo8), 5.33 (Mo9), 6.12 (Mo10), 5.42 (Mo11) and 5.38 (Mo12) for **1**, 5.41 (Mo1), 6.01 (Mo2), 6.12 (Mo3), 5.33 (Mo4), 5.20 (Mo5), 6.04 (Mo6), 5.37 (Mo7), 6.04 (Mo8), 5.31 (Mo9), 5.28 (Mo10), 5.24 (Mo11) and 5.25 (Mo12) for **2**, which confirms the existence of eight Mo^V and four Mo^{VI} in the asymmetric units of **1** and **2**. Further, the distances of Mo^V–Mo^V are 2.6075 to 2.639 Å and Mo^{VI}–Mo^{VI} are 3.174 to 3.1949 Å in **1** and **2**, respectively, also indicating the coexistence of Mo^V and Mo^{VI} ions in **1** and **2**. One can note that to balance the higher negative charge on the Zn_4-capped ε-Keggin skeleton, two protons are added to compounds **1** and **2**, which is common in POM-based compounds.[48]

3.1.1 Structural description of compound 1. The asymmetric unit of **1** contains one $[\varepsilon\text{-}PMo_8{}^{V}Mo_4{}^{VI}O_{40}]$ POM unit, four crystallographically independent Zn^{2+} centers, three Him ligands (one of them is deprotonated), two TBA^+ cations, and three lattice water molecules (Fig. S1†). The four Zn^{2+} ions all have a distorted tetrahedral configuration, of which three oxygen atoms are from the $[\varepsilon\text{-}PMo_8{}^{V}Mo_4{}^{VI}O_{40}]$ POM skeleton (Zn–O: 1.931(11)–1.982(10) Å) and one N atom is from the ligands (Zn–N: 1.922(16)–1.965(13) Å) (Fig. S2†). In compound **1**, the $\{\varepsilon\text{-}PMo_8{}^{V}Mo_4{}^{VI}O_{40}\}$ skeleton is capped by four Zn ions in the tetrahedral symmetry to further construct a secondary building unit (abbreviated as $\mathbf{PMo_{12}Zn_4}$). Each $\mathbf{PMo_{12}Zn_4}$ unit is connected to four Him ligands (two of them are deprotonated and coordinated with Zn1 and Zn2) *via* Zn ions. Benefiting from such a coordination pattern, the $\mathbf{PMo_{12}Zn_4}$ unit is linked to two adjacent $\mathbf{PMo_{12}Zn_4}$ subunits through the protonated imidazole ligands to further form a one-dimension spiral infinite chain (–im–$\mathbf{PMo_{12}Zn_4}$–im–$\mathbf{PMo_{12}Zn_4}$–) with a square-like channel (named channel A) along the direction of the c axis (Fig. 1a–c). Each helical one-dimensional chain interacts with two adjacent chains with opposite chirality through C–H···O and N–H···O hydrogen bonding interactions (D···A: 2.78–3.17 Å) to further stack into a charming 3D supramolecular porous framework (Fig. 1d), which also results in that thus, the entire molecule of **1** is achiral, which is proven by the crystallization of **1** in space group $I4_1/a$. Interestingly, in the 3D framework, a larger square-like channel (named channel B) stacked by four chiral chains (two of which are right-handed) can be viewed from the *c*-axis (Fig. 1c). One should also note that compound **1** eventually presents a channel interpenetrated configuration, that is, there are two types of square-like channels that exist in the direction of the *a*-axis and *b*-axis of the three-dimensional structure (Fig. S4†).

3.1.2 Structural description of compound 2. In optimizing the synthesis conditions of compound **1**, some strip crystals were gradually observed as the pH of the mixture decreased. The lower the pH, the more strip crystals appeared. The single crystal analysis results show that the strip crystal presents a three-dimensional POM-based metal–organic coordination polymer with covalent framework, namely compound **2**. Detailed analysis showed that there are one $[\varepsilon\text{-}PMo_8{}^{V}Mo_4{}^{VI}O_{37}(OH)_3]$ core, four Zn^{2+} cations, one Hip ligand, three Him ligands, one TBA^+ cation and one K^+ ion in the asymmetric unit of compound **2** (Fig. S5†). It should be specifically noted that the 4-(1*H*-imidazol-2-yl)-pyridine (Hip) ligand

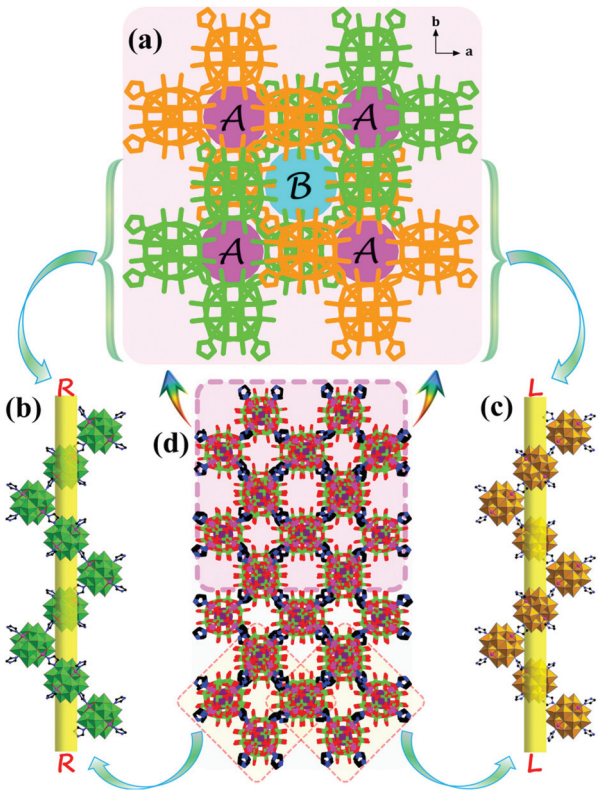

Fig. 1 The structure of compound **1**: (a and b) 1D infinite helical chain constructed from Zn_4-ε-Keggin clusters and imidazole ligands; (c) the channels A and B; (d) the POM-based 3D supramolecular structure. Color code: W, green; {WO_6} octahedron or simplified 1D chain, green or orange; Zn, pink; O, red; N, blue; C, black.

in the final structure was not added to the original raw materials, the presence of which may be caused by the two-molecule decarboxylation reaction of 2-(pyridinium-4-yl)-1*H*-imidazole-4,5-dicarboxylic acid in the hydrothermal environment (Scheme S1†).[49] The four Zn^{2+} cations are crystallographically independent. As shown in Fig. S6,† Zn1 and Zn2 are connected with three oxygen atoms from the ε-Keggin-type POM skeleton (Zn–O: 1.9342(49)–1.9751(54) Å) and one N atom from the ligands (Zn–N: 1.950(73)–1.9828(71) Å) to form a distorted tetrahedral geometry. Zn3 and Zn4 also present a tetrahedral-like geometry by coordinating with four oxygen atoms, of which three O atoms are located on the same POM skeleton, and the remaining O atom comes from the adjacent POM skeleton (Zn–O: 1.9431(54)–1.9866(59) Å). Similarly, there are also Zn_4-capped $\mathbf{PMo_{12}Zn_4}$ secondary building subunits in compound **2**. However, different from compound **1**, each $\mathbf{PMo_{12}Zn_4}$ subunit is linked to two surrounding subunits by four Zn–O bonds (two on each side) to give a one-dimensional zigzag inorganic chain in **2** (Fig. 2a). Such 1D inorganic chains are further connected by two Hip ligands, two K^+ ions and two Him ligands (Zn2–Hip–K^+–2Him–K^+–Hip–Zn2) to form a 2D grid-like layer (Fig. 2b and S7†). Thanks to this double connection mode, the distance between adjacent one-dimensional inorganic chains can reach 17.41 Å (Fig. 2b). Finally, the 3D covalent framework is constructed from the coordination of K^+ ions with the terminal oxygen (O11) located on the ε-Keggin-type POM of the adjacent layer (K–O: 2.0021(2)) (Fig. 2c and d). In the 3D structure, the neighboring 2D layers display staggered stacking, which causes the potential pores in the 2D structure to be blocked by adjacent 2D layers (Fig. 2c). Such a configuration may also be one of the main reasons why compound **2** exhibits relatively poor catalytic activity (compared to compound **1**).

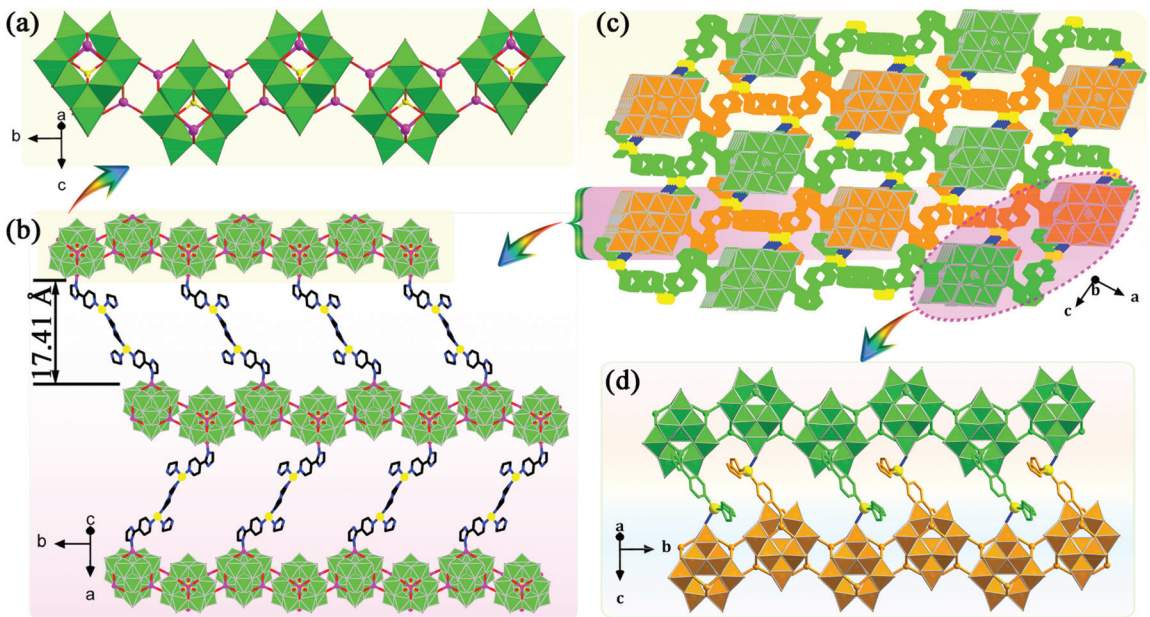

Fig. 2 Structure of compound **2**: (a) the 1D zigzag inorganic chain; (b) the 2D grid-like layer; and (c and d) the 3D covalent framework. Color code: W, green; {WO_6} octahedron or simplified 1D chain, green or orange; Zn, pink; K, yellow; O, red; N, blue; C, black.

3.2 Catalytic performance

3.2.1 Catalytic oxidation of MPS. Owing to the versatility of sulfoxides in organic synthesis, natural products, functional materials, oxygen transfer reagents and biomedicine, the oxidation of sulfides to sulfoxides has attracted the attention of chemists over recent years. Herein, the catalytic behavior of compounds **1** and **2** was first assessed by oxidizing MPS with 30% aqueous H_2O_2 as a green oxidant (Fig. 3a), and screening the optimal operating conditions. As can be seen from Fig. 3b, within 10 min, compound **1** can rapidly achieve >99% substrate conversion, accompanied by almost 100% sulfoxide selectivity under standard conditions ($n_{MPS}:n_{catalyst}:n_{oxidant}$ = 1 : 0.5% : 1.2, 50 °C, 0.5 mL of MeOH). Notably, the catalytic activity expressed in turnover frequency (TOF) reached 1200 h^{-1} and the H_2O_2 utilization efficiency also achieved 90.3%. Although compound **2** also exhibited considerable catalytic activity (>99% MPSO selectivity, 89.5% oxidant utilization efficiency, and 800 h^{-1} TOF) under the same conditions (Fig. 3c), it was still inferior to compound **1**. Benefiting from its well-defined structure, we inferred that the excellent activity of compound **1** may be attributed to its three-dimensional cross channels. Theoretically, larger channels can provide more accessible internal active sites and more efficient mass transfer efficiency.[12,50] It can be seen from the above structural description that the window diameters of the available channels in compound **1** range from 4.8 to 6.6 Å (Fig. S4†), which happen to be able to accommodate the molecular size of MPS (5.3 × 6.2 Å) (Table S3†). Such structural discussion is also consistent with the void space calculated by PLATON. Specifically, compound **1** contains a larger void space (12.4%, 35624.1 $Å^3$ per unit cell) compared to compound **2** (no solvent accessible voids found). Moreover, considering the selectivity of MPSO, TOF and the O/S ratio, the catalysts we synthesized, especially catalyst **1**, are superior to most of the catalytic systems that have been reported thus far (Tables 1 and S4†).[51–58] This series of comparative results suggested that designing porous frameworks with more efficient mass transfer channels and as many exposed active sites as possible may be an efficient strategy by which to build more powerful catalysts.

Additionally, one can note that there are four major factors that play a non-negligible role in the screening of the optimal

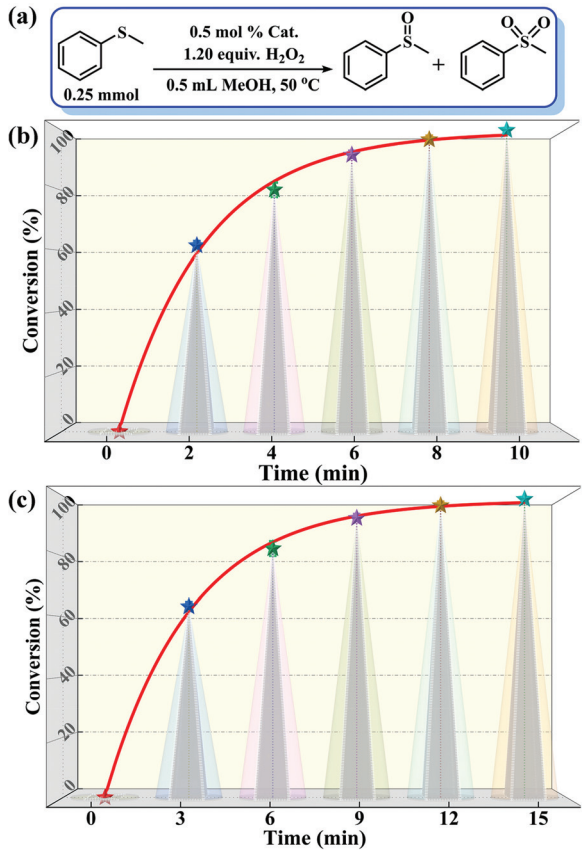

Fig. 3 (a) A schematic diagram of the MPS-MPSO transformation. (b and c) Catalytic results of the MPS-MPSO transformation catalyzed by compounds **1** and **2**.

Table 1 Representative catalytic systems for the oxidation of MPS to MPSO

Catal.[a]	Oxid.	O/S[b]	Time (min)	Conv. (%)	Sel. (%)	TOF (h^{-1})[c]	Ref.
Catalyst 1	H_2O_2	1.2	10	>99	>99	1200	—[d]
Catalyst 2	H_2O_2	1.2	15	>99	>99	800	—[d]
$Cu_8(Mo_8)_2$	TBHP	1.6	30	99	99	198	37
$(Zn_4PMo_{12})_2$	H_2O_2	1.08	30	>99	>99	400	33
$Co(PMo_6)_2$	H_2O_2	1.2	20	99.5	98	298.5	51
$CuTeMo_6$	TBHP	1.1	60	97	99	1616.7	52
$Cu_3Co_2Mo_{10}$	TBHP	2.0	240	99	100	16.5	53
$Zr_{24}Ge_6W_{56}$	H_2O_2	3.0	60	99	16	99	21
$Ru_2As_4W_{40}$	H_2O_2	2.5	60	97.4	87	608.8	54
$V^{IV}{}_8$	TBHP	0.67	480	90	97.8	33.8	55
$V^{V}{}_{17}V^{IV}{}_{12}$	TBHP	2.0	60	98	91	326.7	56
NiV_2	TBHP	1.5	15	100	99	666.7	34
NiV_4	H_2O_2	2.5	60	100	100[e]	20	57
Ni_2V_4	H_2O_2	1.2	240	96.8	98.7	6.9	35
$Co_4Se_8V_{20}$	TBHP	3.0	60	98.9	100	494.5	58

[a] Representative catalyst names only list the metal elements and heteroatoms. [b] O/S = the molar ratio of oxidant to substrate. [c] Turnover frequency (TOF) = (mol of MPS consumed)/(mol of catalyst used × reaction time). [d] This work. [e] Selectivity to $MPSO_2$.

Table 2 The oxidation of MPS to MPSO catalyzed by compound **1**[a]

Entry	Catal. (μmol)	H_2O_2 (mmol)	Temp. (°C)	Time (min)	Con.[b] (%)	Sel.[c] (%)	TOF[d] (h^{-1})
1	1.25	0.30	r.t.	10	36.5	>99	438
2	1.25	0.30	40	10	68.7	>99	824.4
3	**1.25**	**0.30**	**50**	**10**	**>99**	**>99**	**1200**
4	1.25	0.30	60	10	>99	97.5	1200
5	1.25	0.25	50	35	94.8	>99	325
6	1.25	0.35	50	10	>99	94.6	1200
7[e]	1.25	0.30	50	90	94.3	>99	125.7
8[f]	1.25	1 atm	50	120	34.9	>99	34.9
9	1.00	0.30	50	10	97.5	>99	1462.5
10	1.5	0.30	50	10	>99	>99	1000
11	0	0.30	50	30	64.7	79.4	—
12	1.25	0	50	40	28.2	>99	84.6
13	0	0	50	60	Trace	Trace	—

[a] Reaction conditions: 0.25 mmol of MPS and 0.5 mL of MeOH. [b] Results determined *via* GC using naphthalene as an internal standard. [c] Selectivity to MPSO. [d] Turnover frequency (TOF) = (mol of MPS consumed)/(mol of catalyst used × reaction time). [e] TBHP as an oxidant. [f] O_2 as an oxidant.

catalytic conditions (Tables 2 and S3†). Initially, considering that a small change in reaction temperature usually has a great impact on catalytic results, the reaction temperature was determined as the first research variable. As expected, the conversion of MPS can be increased from 36.5% to 100% simply by changing the reaction temperature from room temperature (r.t.) to 50 °C (Table 2, entries 1–3). However, the selectivity of MPSO decreased and the selectivity of the corresponding methyl phenyl sulfone ($MPSO_2$)increased with a further temperature increase (Table 2, entries 3 and 4). Second, the H_2O_2 dosage in the catalytic reactions exhibited a similar trend to temperature. Specifically, within a certain range of H_2O_2 dosages (that is, <1.2 equiv.), the conversion of MPS had a positive correlation with the dosage of H_2O_2 (Table 2, entries 3 and 5), and excessive oxidants would further cause some of the MPSO to be oxidized to $MPSO_2$ (Table 2, entry 6). It should also be noted that slightly more than a stoichiometric amount of oxidant was required for the full conversion of MPS to MPSO (1.0 equiv.), suggesting unproductive decomposition of H_2O_2 under reaction conditions. Although the oxidation of MPS catalyzed by catalyst **1** can also be realized by using *tert*-butyl hydroperoxide or oxygen as an oxidant, the catalyst showed lower catalytic activity (Table 2, entries 7 and 8), which indicated that the active sites on catalyst **1** are more easily activated by hydrogen peroxide. Third, the amount of catalyst is also an important variable that affects catalytic performance, especially the TOF. A low catalyst dosage improved the TOF (up to 1462.5 h^{-1}) but reduced the conversion, while a high catalyst dosage reduced the TOF at full conversion (Table 2, entries 9 and 10). Fourth, alcohol solvents with moderate polarity are conducive to the reaction but too strong a polarity of the solvents (DMF and DMSO) has a negative impact on the reaction (Table S5†). Overall, taking MPS conversion, MPSO selectivity, TOF, and other factors into consideration, the catalytic reaction was carried out at 50 °C in MeOH with an optimal molar ratio of substrate//oxidant catalyst of 1/1.2/0.5% (Table 1, entry 3). Besides this, the control experiments revealed that poor MPS conversion rate and MPSO selectivity were obtained if the catalyst and oxidant were used alone or neither were used (Table 2, entries 11–13).

3.2.2 Substrate scope. With the establishment of the optimal reaction conditions, we then studied the universality of sulfide oxidation catalyzed by the titled compounds. As showed in Scheme 1, MPS and its derivatives with different substituents could be quickly oxidized to the corresponding sulfoxides, with a yield mostly above 90%. It was worth noting that no matter whether the substituents were located in the *ortho*, *meta* or *para* positions of the aromatic ring, the formation of the target products was be affected (Scheme 1, **6a–8a**). In addition, MPS with an electron-withdrawing group or an electron-donating group could also be transformed into the corresponding sulfoxide-based products without excessive oxidation (Scheme 1, **2a–10a**). These excellent catalytic results also indicated that the steric hindrance or electronic factors of the aromatic ring have negligible effects on our catalytic system. Moreover, good to excellent results could also be obtained for sulfides with aromatic heterocycles, such as 2-pyridyl methyl sulfide and 2-methyl-3-methylthiofuran (Scheme 1, **11a–12a**). In addition, other phenyl sulfides with various alkyl or aryl groups substituents such as ethyl, allyl, cyclopropyl, 2-hydroxyethyl, phenyl, and benzyl could also be favorably and efficiently converted to required oxidation products with moderate to excellent yields (Scheme 1, **13a–18a**). Amazingly, catalysts **1** and **2** also showed excellent catalytic activity towards phenoxathiine and dibenzyl sulfide, and high yields could be obtained in a short time (Scheme 1, **19a–20a**). In terms of aliphatic sulfides, the corresponding sulfoxides with high yield could be obtained in a shorter time compared with aromatic sulfides (Scheme 1, **21a–24a**). One can note that the oxidation of various sulfides catalyzed by compound **1** also showed better activity than compound **2** as a whole, which further proved that the porous framework of compound **1** was more conducive to the catalytic reaction.

3.2.3 Catalytic oxidative detoxification of CEES. Despite chemical warfare agents being banned in principle worldwide, the threat of their use as terrorist weapons will long persist.[59]

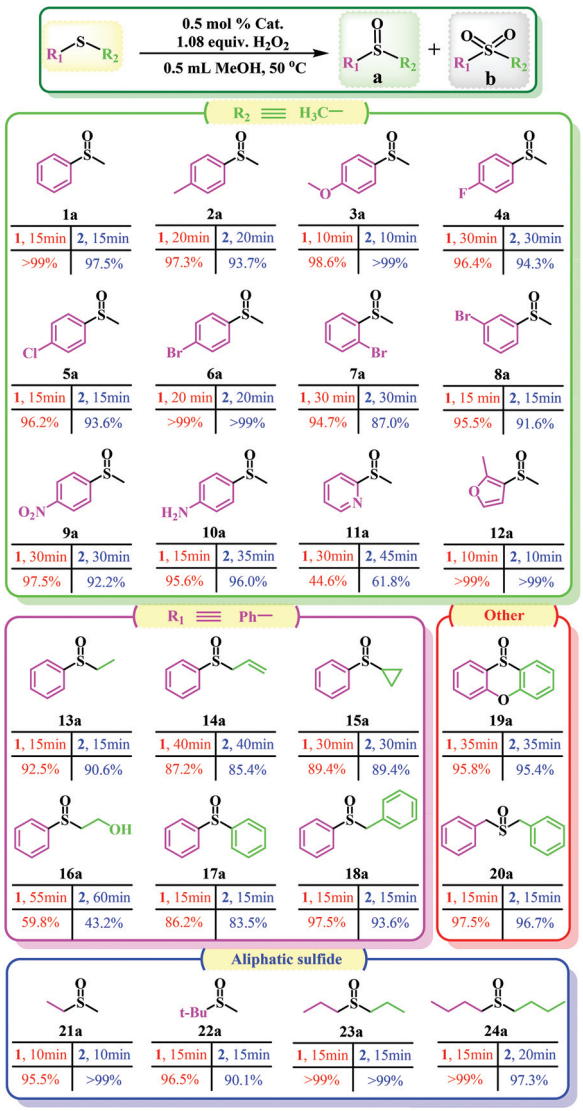

Scheme 1 Results for compounds **1** and **2** catalyzing the oxidation of various sulfide substrates.

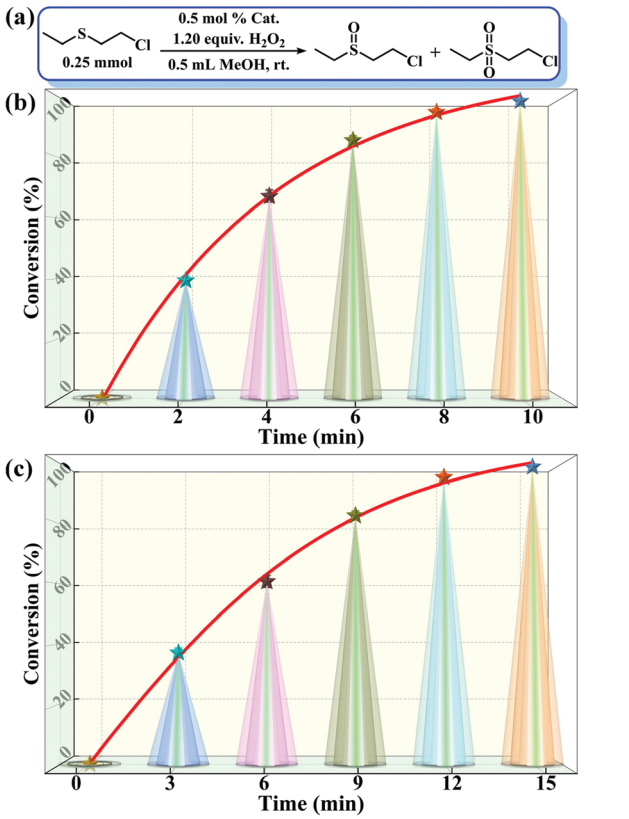

Fig. 4 (a) The oxidation detoxification of CEES to CEESO or $CEESO_2$. (b and c) The transformation of CEES using **1** and **2** as catalysts.

Among them, sulfur mustard, one of the most vicious foaming agents, is still used in wars or terrorist attacks due to its ease of synthesis and transmission, and has ended thousands of lives.[59] Therefore, the development of highly effective preventative and therapeutic measures for deactivating sulfur mustard is an area of high importance. In recent decades, the selective oxidation of sulfur mustard to non-toxic bis-2-chloroethyl sulfoxide (note that the corresponding sulfone is toxic) has been extensively studied as a promising degradation pathway. In view of the high-efficiency selectivity towards sulfoxides of the title catalysts, herein, 2-chloroethyl ethyl sulfide (CEES, an effective simulant of sulfur mustard) was chosen as a research object to evaluate the catalytic performance of compounds **1** and **2** in CEES degradation (Fig. 4a). The catalytic reaction conditions were basically the same as the oxidation of MPS, except that the reaction was carried out at room temperature ($n_{CEES} : n_{catalyst} : n_{oxidant}$ = 1 : 0.5% : 1.2, r.t., 0.5 mL of MeOH). As predicted, both compounds **1** and **2** showed outstanding activity and selectivity towards the catalytic detoxification of CEES. Specifically, within 10–15 min, CEES was completely converted into the corresponding non-toxic CEESO with >99% selectivity (Fig. 4b and c). The H_2O_2 utilization efficiencies were also as high as 94.5% for **1** and 92.7% for **2**. Similar to the above trend in the oxidation of MPS, compound **1** also showed better catalytic activity in the detoxification of CEES compared to **2**.

3.2.4 Catalyst sustainability and stability. Sustainability and stability are crucial indicators to evaluate whether a catalyst holds potential for practical application. Primarily, we utilized a simple hot filtration method to judge the heterogeneous nature of the catalysts. As can be seen from Fig. 5a, catalyst **1** was rapidly filtered out when the mixture was reacted for 2 min under standard conditions, and the conversion of MPS was basically constant after the remaining filtrate continued to react in the initial environment for a further 8 min, which illustrated the excellent heterogeneity of the catalyst. Moreover, similar conclusions can be further verified by the fact that there were no characteristic absorption peaks of ε-Keggin skeleton in the full spectrum range of the liquid UV-vis spectrum of the filtrate after the reaction (Fig. S11a†). We then went through a cycling experiment by simply filtering out the catalyst **1** after one cycle of the MPS oxidation reaction. The

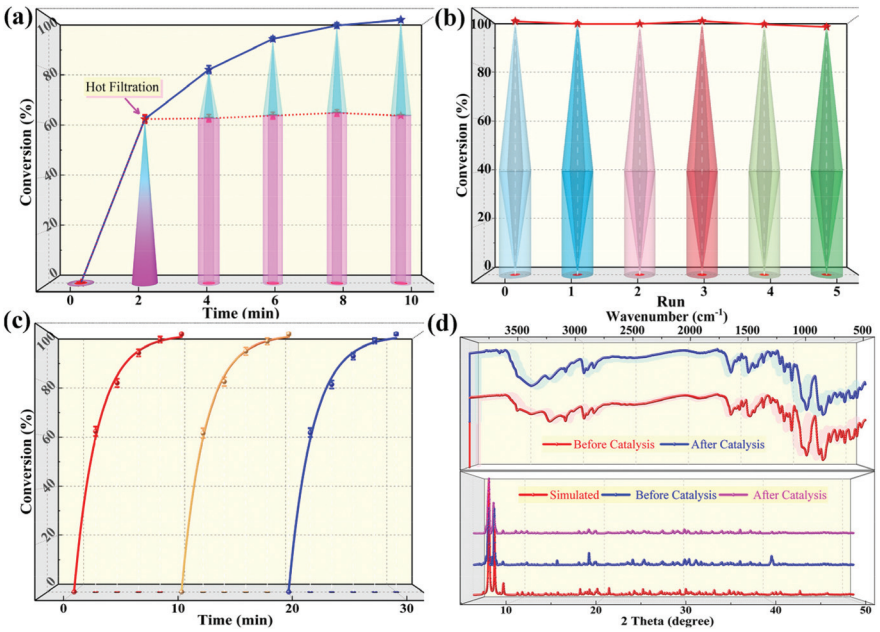

Fig. 5 (a) Hot filtration experiment using **1** for the catalytic oxidation of MPS. (b) Cycling experiments involving the oxidation of MPS using spent **1**. (c) Continuous cycling experiments involving the oxidation of MPS using **1**. (d) The FTIR spectra and PXRD patterns of fresh and spent catalyst **1**.

results showed that the conversion of MPS remained at the same level as that of fresh catalyst, and the conversion did not decrease significantly with an increase in the number of cycles (Fig. 5b). Also, the subsequent continuous cycling experiment also revealed that the catalytic activity of **1** showed no obvious changes after three consecutive cycles of testing (Fig. 5c). Importantly, the Fourier-transform infrared (FTIR) spectra and powder X-ray diffractometry (PXRD) patterns of the fresh and spent catalyst **1** are highly consistent, which proves the structural stability of the catalyst (Fig. 5d). In addition, similar conclusions could also be easily interpreted in the MPS oxidation catalyzed by catalyst **2**, as well as the detoxification of CEES catalyzed by catalysts **1** and **2** (Fig. S11–S15†). These results indicated that the selective oxidation of sulfides to sulfoxides over the title catalysts showed high catalytic activity, with the catalysts also exhibiting excellent stability under optimal conditions.

3.2.5 Kinetics study. To better understand the kinetic behavior of the above catalytic system, the oxidation of MPS and the oxidative detoxification of CEES catalyzed by compounds **1** and **2** were monitored in real time under the optimal conditions. For the sake of brevity, the following detailed discussion only takes the oxidation of MPS catalyzed by compound **1** as an example. As shown in Fig. S16,† the conversion of MPS and the natural logarithm ($\ln(C_t/C_0)$) of the ratio of the initial concentration (C_0) of MPS to the concentration at a given time (C_t) was plotted against the reaction time at 50 °C. The linear fitting results showed that such a catalytic system might undergo a pseudo first-order kinetic process (R^2 = 0.9941), and that the observed rate constant (k) of **1** at 50 °C was 0.4493 min^{-1}. Similar linear fittings were also carried out for the time-conversion curves at 40 °C and 45 °C. The results revealed that both **1** and **2** exhibited pseudo-first-order kinetic characteristics (R^2 = 0.9983 and k = 0.1294 min^{-1} for 40 °C, and R^2 = 0.9895 and k = 0.2160 min^{-1} for 45 °C, respectively) (Fig. 6a). Based on the above data, the activation energy (E_a) of the oxidation of MPS catalyzed by compound **1** was calculated from the Arrhenius equation as 95.16 kJ mol^{-1}, which indicated that the oxidation of MPS was not restricted by diffusion in this catalytic system (Fig. 6b and Table S6†). Besides this, the corresponding activation enthalpy ($\Delta H^{\neq}$) and activation entropy ($\Delta S^{\neq}$) calculated from the Eyring equation under the optimal conditions were 92.47 kJ mol^{-1} and 6.56 J mol^{-1} K^{-1} (Table S6†). The above conclusions were also applicable to the MPS conversion catalyzed by compound **2**, that is, the catalytic system also exhibited the same quasi-first-order kinetic status in the range of 40 to 50 °C (Fig. S17†), and the calculated relevant data are listed in Table S5.† Of particular note is that the E_a of compound **2** (100.64 kJ mol^{-1}) was slightly higher than that of compound **1**, indicating that the oxidation of MPS is easier to carry out in the presence of **1** under the same conditions. Similarly, we also conducted kinetic studies on the catalytic degradation systems of CEES, and the results showed that they also exhibited first-order kinetic behavior (Fig. S18 and S19†).

3.2.6 Possible mechanism. Primarily, before clarifying the possible reaction mechanism, a question remains to be answered: what are the real active centers? As shown in Table 3, a series of indirect detection control experiments for the oxidation of MPS were carried out under standard conditions. GC analysis of the comparative experiment with pure H_3PO_3 and Him showed that the conversion of MPS could still

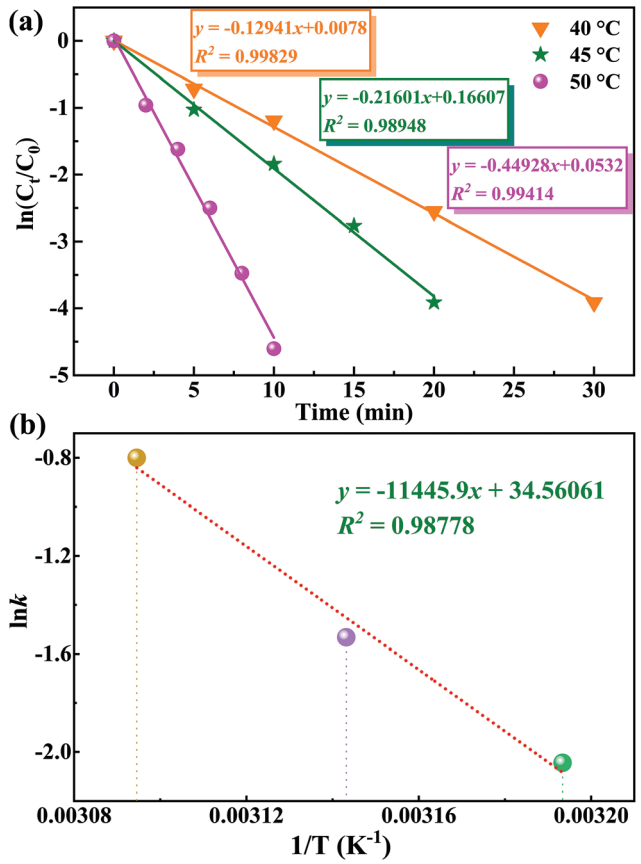

Fig. 6 (a) The kinetic profiles of the oxidation of MPS catalyzed by compound **1** at 40 °C, 45 °C, and 50 °C. (b) The Arrhenius–Eyring plot ($\ln k = -(E_a/RT) + \ln A$).

reach 50%, and that the yield of MPSO was close to 45% (Table 3, entries 1 and 2), but this result may be mainly attributed to the efficacy of the oxidant itself (Table 2, entry 11). Moreover, the catalytic result with the addition of pure $Zn(Ac)_2$ was slightly better than that of the absence of any catalyst, which also illustrated that the role of Zn ions in the oxidation reaction is weak (Table 3, entry 3). While $(NH_4)_6Mo_7O_{24}{\cdot}4H_2O$ (abbreviated as Mo_7) and $[TBA]_4[\varepsilon\text{-}PMo^{V}{}_8Mo^{VI}{}_4O_{37}(OH)_3Zn_4]Cl_4$ (the pure inorganic ε-Keggin POM,[60] abbreviated as $\{PMo_{12}Zn_4\}$) were active for the oxidation of MPS, giving 94% to 98% conversion, the corresponding MPSO selectivity (~85% for both) was not very satisfactory, and the TOF calculated based on MPSO yield was 2.4-fold lower than that of compound **1** (Table 3, entries 4 and 5). Furthermore, running the experiment with a simple physical mixture of $\{PMo_{12}Zn_4\}$/Him as a catalyst under the optimal conditions also manifested in a catalytic result inferior to that of compound **1** (Table 3, entries 6 and 7). Although the 3D compound **2** also showed a higher catalytic activity than the simple mixture, it remained significantly lower than that of compound **1** (Table 3, entry 8). These results not only indicate that the active centers of **1** may be located on the Mo of the ε-Keggin POM skeleton, but also further demonstrate that the structural microenvironment of compound **1** has an important influence on catalysis.

Based on the above results, we identified the Mo ions on the POM as the active centers of the reaction. In addition, from a structural viewpoint, it is known that the outermost layer of the pseudo-spherical ε-Keggin POM is coordinated with 12 active terminal oxygen atoms, which means that these sites are readily activated in the reaction and ensures that there are potential Mo sites interacting with H_2O_2 to form active intermediates (namely, peroxo-POMs).[23] This speculation was further supported by the spectral characterization. The characteristic absorption peak of the POM skeleton shifted to a longer wavelength (red-shift) in the liquid phase UV-vis spectra after adding several drops of H_2O_2 into DMSO solutions of compounds **1** and **2**, indicating a change in the coordination environment on the Mo atoms, namely the formation of active peroxymolybdates (Fig. 7a and S20†). The active species could be further identified from solid Raman spectra and a new peak was present at 750 cm^{-1} after the catalysts were treated with aqueous hydrogen peroxide (Fig. S21†). Moreover, in order to eliminate a possible free radical mechanism, the addition of free radical scavengers (such as isopropanol, diphenylamine and *p*-benzoquinone) in the reaction system could not effectively prevent the formation of MPSO, indicating that reactive oxygen radicals such as hydroxyl and superoxide radicals do not participate in the oxidation of MPS. Out of these results, a plausible catalytic cycle for the sulfide–

Table 3 Activities of different catalysts towards the oxidation of MPS[a]

Entry	Cat.	Time (min)	Con. (%)	Yield[b] (%)	TOF[c] (h^{-1})	Reaction system
1	H_3PO_3	35	49.8	41.9	143.7	Homogeneous
2	Him	30	50.2	44.8	59.77	Homogeneous
3	$Zn(Ac)_2$	30	68.3	53.3	53.3	Homogeneous
4	Mo_7	20	97.6	85.1	296.9	Homogeneous
5	$PMo_{12}Zn_4$	20	94.5	81.0	486	Homogeneous
6[d]	Mix.	40	84.9	82.7	62	Homogeneous
7	**1**	10	>99	>99	1200	Heterogeneous
8	**2**	15	>99	>99	800	Heterogeneous

[a] Reaction conditions: 0.25 mmol of MPS; 0.30 mmol of H_2O_2; 50 °C, 0.5 mol% **1** and **2** (molar amounts of other catalysts were added according to the formula of compound **1**). [b] Yield to MPSO. [c] TOF = (mol of MPS generated)/(mol of catalyst used × reaction time). [d] Simple physical mixture of $PMo_{12}Zn_4$ and Him.

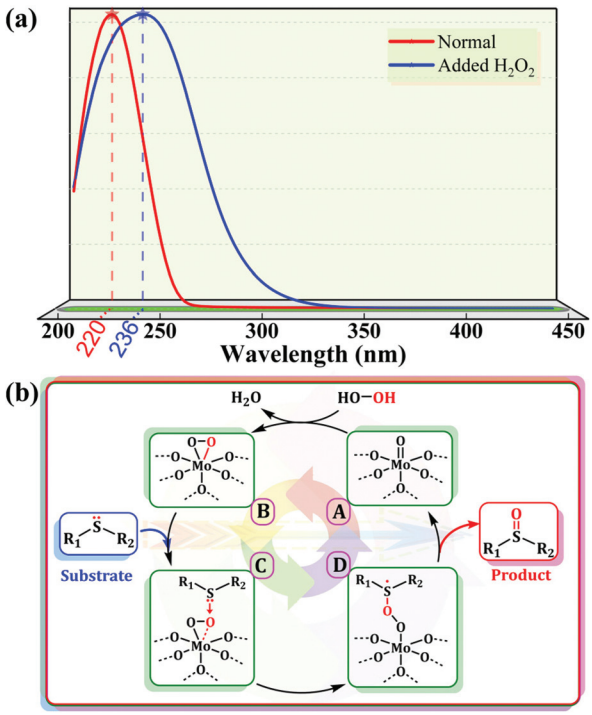

Fig. 7 (a) UV-vis spectra of **1** before and after treatment with H_2O_2. (b) A mechanistic diagram of MPS or CEES oxidation.

sulfoxide transformation comes into view clearly (Fig. 7b). In the first stage of the catalytic oxidation process, the terminal metal–oxygen groups (Mo=O_t) in the POM skeleton first react with hydrogen peroxide to form electrophilic peroxide species (**B**). Subsequently, the nucleophilic sulfur atom in the sulfide attacks **B** to produce the unstable intermediate (**D**), which rapidly releases the corresponding sulfoxide and the original form of the POM groups is reinstated to complete the catalytic cycle.

4. Conclusions

Briefly, we designed and synthesized a robust heterogeneous catalyst based on a porous POM-based supramolecular framework. The as-prepared catalyst can efficiently oxidize a variety of substituted phenyl or aliphatic sulfides to the corresponding sulfoxides with high catalytic activity. In particular, in the oxidation of MPS, almost 100% MPSO yield was achieved at a low O/S ratio within 10 min. The corresponding TOF was also up to 1200 h^{-1}, which was obviously higher than that of compound **2** (800 h^{-1}), a 3D analogous covalent framework. Structure–activity analysis showed that the excellent catalytic activity of compound **1** stems from its porous framework, which promotes an efficient mass transfer process and more accessible internal active sites. More importantly, there was no significant decrease in activity after 5 cycles, indicating that the title catalyst possessed excellent sustainability and stability. This work not only contributes towards broadening catalyst systems for the study of sulfide oxidation, but it also opens up an avenue for the design of highly active POM-based heterogeneous catalysts for sulfide-sulfoxide transformations.

Author contributions

Yanhong Chen participated in the main work of the manuscript, including designing the project, synthesizing, characterizing, and testing the catalysts, and writing the original draft. Shenzhen Chang helped with catalytic performance testing, analysing data, drawing graphs, and reviewing and editing the manuscript. Qingshan Zhu, Huiyun Luo, and Yaohui Huang assisted with reviewing and editing the manuscript. Haiyan An and Yanqin Li supervised and provided helpful discussion, and revised the manuscript.

Conflicts of interest

The authors declare that they have no known competing financial interests or personal relationships that could have appeared to influence the work reported in this paper.

Acknowledgements

This work was financially supported by the National Natural Science Foundation of China (21371027, 20901013), the Natural Science Foundation of Liaoning Province (2015020232), and the Fundamental Research Funds for the Central Universities (DUT19LK01, DUT15LN18).

References

1 K. Kamata, K. Sugahara, Y. Kato, S. Muratsugu, Y. Kumagai, F. Oba and M. Hara, Heterogeneously catalyzed aerobic oxidation of sulfides with a $BaRuO_3$ nanoperovskite, *ACS Appl. Mater. Interfaces*, 2018, **10**, 23792–23801.
2 T. Ishizuka, S. Ohkawa, H. Ochiai, M. Hashimoto, K. Ohkubo, H. Kotani, M. Sadakane, S. Fukuzumi and T. Kojima, A supramolecular photocatalyst composed of a polyoxometalate and a photosensitizing water-soluble porphyrin diacid for the oxidation of organic substrates in water, *Green Chem.*, 2018, **20**, 1975–1980.
3 P. Mialane, C. Mellot-Draznieks, P. Gairola, M. Duguet, Y. Benseghir, O. Oms and A. Dolbecq, Heterogenisation of polyoxometalates and other metal-based complexes in metal–organic frameworks: from synthesis to characterisation and applications in catalysis, *Chem. Soc. Rev.*, 2021, **50**, 6152–6220.
4 K.-J. Liu, J.-H. Deng, J. Yang, S.-F. Gong, Y.-W. Lin, J.-Y. He, Z. Cao and W.-M. He, Selective oxidation of (hetero)sulfides with molecular oxygen under clean conditions, *Green Chem.*, 2020, **22**, 433–438.

5 M. Cao, R. Pang, Q. Y. Wang, Z. Han, Z. Y. Wang, X. Y. Dong, S. F. Li, S. Q. Zang and T. C. W. Mak, Porphyrinic silver cluster assembled material for simultaneous capture and photocatalysis of mustard-gas simulant, *J. Am. Chem. Soc.*, 2019, **141**, 14505–14509.

6 J. Song, Y. Li, P. Cao, X. Jing, M. Faheem, Y. Matsuo, Y. Zhu, Y. Tian, X. Wang and G. Zhu, Synergic catalysts of polyoxometalate@cationic porous aromatic frameworks: reciprocal modulation of both capture and conversion materials, *Adv. Mater.*, 2019, **31**, e1902444.

7 X. Li, J. Dong, H. Liu, X. Sun, Y. Chi and C. Hu, Recoverable amphiphilic polyoxoniobates catalyzing oxidative and hydrolytic decontamination of chemical warfare agent simulants in emulsion, *J. Hazard. Mater.*, 2018, **344**, 994–999.

8 M. Ahmadian and M. Anbia, Oxidative desulfurization of liquid fuels using polyoxometalate-based catalysts: a review, *Energy Fuels*, 2021, **35**, 10347–10373.

9 S. Wang, L. Wang, M. Đaković, Z. Popović, H. Wu and Y. Liu, Bifunctional ionic liquid catalyst containing sulfoacid group and hexafluorotitanate for room temperature sulfoxidation of sulfides to sulfoxides using hydrogen peroxide, *ACS Catal.*, 2012, **2**, 230–237.

10 C. Xu, Y. Pan, G. Wan, H. Liu, L. Wang, H. Zhou, S. H. Yu and H. L. Jiang, Turning on visible-light photocatalytic C–H oxidation over metal-organic frameworks by introducing metal-to-cluster charge transfer, *J. Am. Chem. Soc.*, 2019, **141**, 19110–19117.

11 S. Mazzanti, G. Manfredi, A. J. Barker, M. Antonietti, A. Savateev and P. Giusto, Carbon nitride thin films as all-in-one technology for photocatalysis, *ACS Catal.*, 2021, **11**, 11109–11116.

12 S. Z. Chang, Y. H. Chen, H. Y. An, Q. S. Zhu, H. Y. Luo and Y. H. Huang, Polyoxometalate-based supramolecular porous frameworks with dual-active centers towards highly efficient synthesis of functionalized p-benzoquinones, *Green Chem.*, 2021, **23**, 8591–8603.

13 A. Atilgan, M. M. Cetin, J. Yu, Y. Beldjoudi, J. Liu, C. L. Stern, F. M. Cetin, T. Islamoglu, O. K. Farha, P. Deria, J. F. Stoddart and J. T. Hupp, Post-synthetically elaborated BODIPY-based porous organic polymers (POPs) for the photochemical detoxification of a sulfur mustard simulant, *J. Am. Chem. Soc.*, 2020, **142**, 18554–18564.

14 J. C. Liu, J. F. Wang, Q. Han, P. Shangguan, L. L. Liu, L. J. Chen, J. W. Zhao, C. Streb and Y. F. Song, Multicomponent self-assembly of a giant heterometallic polyoxotungstate supercluster with antitumor activity, *Angew. Chem., Int. Ed.*, 2021, **60**, 11153–11157.

15 N. V. Maksimchuk, G. M. Maksimov, V. Y. Evtushok, I. D. Ivanchikova, Y. A. Chesalov, R. I. Maksimovskaya, O. A. Kholdeeva, A. Solé-Daura, J. M. Poblet and J. J. Carbó, Relevance of protons in heterolytic activation of H_2O_2 over Nb(V): insights from model studies on Nb-substituted polyoxometalates, *ACS Catal.*, 2018, **8**, 9722–9737.

16 J. Liu, W. Shi and X. Wang, ZnO-POM cluster sub-1 nm nanosheets as robust catalysts for the oxidation of thioethers at room temperature, *J. Am. Chem. Soc.*, 2021, **143**, 16217–16225.

17 X.-H. Li, W.-L. Chen, P. He, T. Wang, D. Liu, Y.-W. Li, Y.-G. Li and E.-B. Wang, Dawson-type polyoxometalate-based vacancies g-C_3N_4 composite-nanomaterials for efficient photocatalytic nitrogen fixation, *Inorg. Chem. Front.*, 2019, **6**, 3315–3326.

18 S. Z. Chang, Y. H. Chen, H. Y. An, Q. S. Zhu, H. Y. Luo and T. Q. Xu, Highly efficient synthesis of p-benzoquinones catalyzed by robust two-dimensional POM-based coordination polymers, *ACS Appl. Mater. Interfaces*, 2021, **13**, 21261–21271.

19 S. Zhang, N. Liu, H. Wang, Q. Lu, W. Shi and X. Wang, Sub-nanometer nanobelts based on titanium dioxide/zirconium dioxide-polyoxometalate heterostructures, *Adv. Mater.*, 2021, **33**, e2100576.

20 C. Li, N. Mizuno, K. Murata, K. Ishii, T. Suenobu, K. Yamaguchi and K. Suzuki, Selectivity switch in the aerobic oxygenation of sulfides photocatalysed by visible-light-responsive decavanadate, *Green Chem.*, 2020, **22**, 3896–3905.

21 L. Huang, S. S. Wang, J. W. Zhao, L. Cheng and G. Y. Yang, Synergistic combination of multi-Zr(IV) cations and lacunary keggin germanotungstates leading to a gigantic Zr_{24}-cluster-substituted polyoxometalate, *J. Am. Chem. Soc.*, 2014, **136**, 7637–7642.

22 C. Yang, Q. Jin, H. Zhang, J. Liao, J. Zhu, B. Yu and J. Deng, Tetra-(tetraalkylammonium)octamolybdate catalysts for selective oxidation of sulfides to sulfoxides with hydrogen peroxide, *Green Chem.*, 2009, **11**, 1401–1405.

23 J. Dong, J. F. Hu, Y. N. Chi, Z. G. Lin, B. Zou, S. Yang, C. L. Hill and C. W. Hu, A polyoxoniobate-polyoxovanadate double-anion catalyst for simultaneous oxidative and hydrolytic decontamination of chemical warfare agent simulants, *Angew. Chem., Int. Ed.*, 2017, **56**, 4473–4477.

24 T. A. G. Duarte, S. M. G. Pires, I. C. M. S. Santos, M. M. Q. Simões, M. G. P. M. S. Neves, A. M. V. Cavaleiro and J. A. S. Cavaleiro, A Mn(III) polyoxotungstate in the oxidation of organosulfur compounds by H_2O_2 at room temperature: an environmentally safe catalytic approach, *Catal. Sci. Technol.*, 2016, **6**, 3271–3278.

25 I. Y. Skobelev, O. V. Zalomaeva, O. A. Kholdeeva, J. M. Poblet and J. J. Carbo, Mechanism of thioether oxidation over di- and tetrameric ti centres: kinetic and DFT studies based on model Ti-containing polyoxometalates, *Chem. – Eur. J.*, 2015, **21**, 14496–14506.

26 W. Jiang, J. Xiao, L. Dong, C. Wang, H. Li, Y. Luo, W. Zhu and H. Li, Polyoxometalate-based poly(ionic liquid) as a precursor for superhydrophobic magnetic carbon composite catalysts toward aerobic oxidative desulfurization, *ACS Sustainable Chem. Eng.*, 2019, **7**, 15755–15761.

27 Z. Yao, H. N. Miras and Y.-F. Song, Efficient concurrent removal of sulfur and nitrogen contents from complex oil mixtures by using polyoxometalate-based composite materials, *Inorg. Chem. Front.*, 2016, **3**, 1007–1013.

28 J. P. Cao, Y. S. Xue, N. F. Li, J. J. Gong, R. K. Kang and Y. Xu, Lewis acid dominant windmill-shaped V_8 clusters: a

bifunctional heterogeneous catalyst for CO_2 cycloaddition and oxidation of sulfides, *J. Am. Chem. Soc.*, 2019, **141**, 19487–19497.

29 A. Rezaeifard, R. Haddad, M. Jafarpour and M. Hakimi, $\{Mo_{132}\}$ nanoball as an efficient and cost-effective catalyst for sustainable oxidation of sulfides and olefins with hydrogen peroxide, *ACS Sustainable Chem. Eng.*, 2014, **2**, 942–950.

30 Y. Guo, J. W. Fu, L. Li, X. N. Li, H. Y. Wang, W. W. Ma and H. Zhang, One-pot synthesis of polyoxomolybdate anion intercalated layered double hydroxides and their application in ultra-deep desulfurization of fuels under mild conditions, *Inorg. Chem. Front.*, 2018, **5**, 2205–2210.

31 S. Zhang, F. Ou, S. Ning and P. Cheng, Polyoxometalate-based metal–organic frameworks for heterogeneous catalysis, *Inorg. Chem. Front.*, 2021, **8**, 1865–1899.

32 H. R. Tian, Z. Zhang, T. Y. Dang, S. M. Liu, Y. Lu and S. X. Liu, Hollow Lindqvist-like-shaped $\{V_6\}$ cluster-based metal-organic framework for the highly efficient detoxification of mustard gas simulant, *Inorg. Chem.*, 2021, **60**, 840–845.

33 Y. Chen, S. Chang, H. An, Y. Li, Q. Zhu, H. Luo and Y. Huang, Two polymorphic polyoxometalate-based metal–organic frameworks for the efficient synthesis of functionalized sulfoxides and detoxification of mustard gas simulants, *ACS Sustainable Chem. Eng.*, 2021, **9**, 15683–15693.

34 X. Wang, T. Zhang, Y. H. Li, J. F. Lin, H. Li and X. L. Wang, In situ ligand-transformation-involved synthesis of inorganic-organic hybrid polyoxovanadates as efficient heterogeneous catalysts for the selective oxidation of sulfides, *Inorg. Chem.*, 2020, **59**, 17583–17590.

35 J. Li, C. Wei, D. Guo, C. Wang, Y. Han, G. He, J. Zhang, X. Huang and C. Hu, Inorganic-organic hybrid polyoxovanadates based on $[V_4O_{12}]^{4-}$ or $[VO_3]^{22-}$ clusters: controllable synthesis, crystal structures and catalytic properties in selective oxidation of sulfides, *Dalton Trans.*, 2020, **49**, 14148–14157.

36 J. Li, X. Huang, S. Yang, Y. Xu and C. Hu, Controllable synthesis, characterization, and catalytic properties of three inorganic–organic hybrid copper vanadates in the highly selective oxidation of sulfides and alcohols, *Cryst. Growth Des.*, 2015, **15**, 1907–1914.

37 X. L. Wang, J. Y. Zhang, Z. H. Chang, Z. Zhang, X. Wang, H. Y. Lin and Z. W. Cui, α–γ-Type $[Mo_8O_{26}]^{4-}$-containing metal–organic complex possessing efficient catalytic activity toward the oxidation of thioether derivatives, *Inorg. Chem.*, 2021, **60**, 3331–3337.

38 Z. G. Jiang, W. T. Mao, D. P. Huang, Y. Wang, X. J. Wang and C. H. Zhan, A nonconventional host-guest cubic assembly based on gamma-cyclodextrin and a Keggin-type polyoxometalate, *Nanoscale*, 2020, **12**, 10166–10171.

39 L. G. Qiu, A. J. Xie and L. D. Zhang, Encapsulation of catalysts in supramolecular porous frameworks: size- and shape-selective catalytic oxidation of phenols, *Adv. Mater.*, 2005, **17**, 689–692.

40 X. Fang, P. Kogerler, L. Isaacs, S. Uchida and N. Mizuno, Cucurbit[n]uril-polyoxoanion hybrids, *J. Am. Chem. Soc.*, 2009, **131**, 432–433.

41 Y.-Q. Jiao, M.-T. Li, C. Qin and Z.-M. Su, A noncovalently connected metal–organic framework assembled from a Ni(III)-supported polyoxometalate–imidazolate hybrid, *CrystEngComm*, 2017, **19**, 1721–1724.

42 Z. Weng, N. Ogiwara, T. Kitao, Y. Kikukawa, Y. Gao, L. Yan and S. Uchida, Incorporating highly basic polyoxometalate anions comprising Nb or Ta into nanoscale reaction fields of porous ionic crystals, *Nanoscale*, 2021, **13**, 18451–18457.

43 M. Stuckart and K. Y. Monakhov, Polyoxometalates as components of supramolecular assemblies, *Chem. Sci.*, 2019, **10**, 4364–4376.

44 C. Zou, Z. Zhang, X. Xu, Q. Gong, J. Li and C. D. Wu, A multifunctional organic-inorganic hybrid structure based on Mn(III)-porphyrin and polyoxometalate as a highly effective dye scavenger and heterogenous catalyst, *J. Am. Chem. Soc.*, 2012, **134**, 87–90.

45 X. Xia, W. W. Ge, H. Chen, Z. Tao, Y. Zhang, G. Wei and K. Chen, Porous supramolecular assemblies and functional properties of perhydroxylated cucurbit[6]uril and polyoxometallates, *New J. Chem.*, 2019, **43**, 10297–10304.

46 Q. Liu, H. Lin, X.-L. Wang, X. Wang, N. Xu, Y. Tian, L. Yang, X. Li and J. Sun, Two novel polyoxometalate-based metal–organic complexes with chiral waugh-type $[MnMo_9O^{32}]^{6-}$ anions as high-efficiency catalytic oxidative desulfurization catalysts, *Cryst. Growth Des.*, 2021, **21**, 7015–7022.

47 I. D. Brown and D. Altermatt, Bond-valence parameters obtained from a systematic analysis of the inorganic crystal structure database, *Acta Crystallogr., Sect. B: Struct. Sci.*, 1985, **41**, 244–247.

48 W. W. Cheng, F. C. Shen, Y. S. Xue, X. M. Luo, M. Fang, Y. Q. Lan and Y. Xu, A pair of rare three-dimensional chiral polyoxometalate-based metal-organic framework enantiomers featuring superior performance as the anode of lithium-ion battery, *ACS Appl. Energy Mater.*, 2018, **1**, 4931–4938.

49 D. D. Li, Q. F. Xu, Y. G. Li, Y. T. Qiu, P. T. Ma, J. Y. Niu and J. P. Wang, A stable polyoxometalate-based metal-organic framework as highly efficient heterogeneous catalyst for oxidation of alcohols, *Inorg. Chem.*, 2019, **58**, 4945–4953.

50 D. Dutta, A. D. Jana, M. Debnath, A. Bhaumik, J. Marek and M. Ali, Robust 1D open rack-like architecture in coordination polymers of Anderson POMs $[\{Na_4(H_2O)_{14}\}\{Cu(gly)\}_2][TeMo_6O_{24}]$ and $[\{Cu(en)_2\}_3\{TeW_6O_{24}\}]$: synthesis, characterization and heterogeneous catalytic epoxidation of olefines, *Dalton Trans.*, 2010, **39**, 11551–11559.

51 H. An, Y. Hou, S. Chang, J. Zhang and Q. Zhu, Highly efficient oxidation of various thioethers catalyzed by organic ligand-modified polyoxomolybdates, *Inorg. Chem. Front.*, 2020, **7**, 169–176.

52 Q. Xu, X. Liang, B. Xu, J. Wang, P. He, P. Ma, J. Feng, J. Wang and J. Niu, 36-Nuclearity organophosphonate-functionalized polyoxomolybdates: synthesis, characterization

and selective catalytic oxidation of sulfides, *Chem. – Eur. J.*, 2020, **26**, 14896–14902.

53 H. Y. An, Y. J. Hou, L. Wang, Y. M. Zhang, W. Yang and S. Z. Chang, Evans-Showell-type polyoxometalates constructing high-dimensional inorganic-organic hybrid compounds with copper-organic coordination complexes: synthesis and oxidation catalysis, *Inorg. Chem.*, 2017, **56**, 11619–11632.

54 M. Han, Y. Niu, R. Wan, Q. Xu, J. Lu, P. Ma, C. Zhang, J. Niu and J. Wang, A crown-shaped Ru-Substituted arsenotungstate for selective oxidation of sulfides with hydrogen peroxide, *Chem. – Eur. J.*, 2018, **24**, 11059–11066.

55 J. Tang, P. F. Yao, X. L. Xu, H. Y. Li, F. P. Huang, Q.-Q. Nie, M. Y. Luo, Q. Yu and H. D. Bian, Asymmetric catalytic sulfoxidation by a novel V^{IV}_8 cluster catalyst in the presence of serum albumin: a simple and green oxidation system, *RSC Adv.*, 2016, **6**, 44154–44162.

56 K. Wang, Y. Niu, D. Zhao, Y. Zhao, P. Ma, D. Zhang, J. Wang and J. Niu, The polyoxovanadate-based carboxylate derivative $K_6H[V^{V}_{17}V^{IV}_{12}(OH)_4O_{60}(OOC(CH_2)_4COO)_8]$ nH_2O: synthesis, crystal structure, and catalysis for oxidation of sulfides, *Inorg. Chem.*, 2017, **56**, 14053–14059.

57 T. Y. Dang, R.-H. Li, H. R. Tian, Q. Wang, Y. Lu and S. X. Liu, Tandem-like vanadium cluster chains in a polyoxovanadate-based metal–organic framework for efficient catalytic oxidation of sulfides, *Inorg. Chem. Front.*, 2021, **8**, 4367–4375.

58 R. Wan, P. He, Z. Liu, X. Ma, P. Ma, V. Singh, C. Zhang, J. Niu and J. Wang, A lacunary polyoxovanadate precursor and transition-metal-sandwiched derivatives for catalytic oxidation of sulfides, *Chem. – Eur. J.*, 2020, **26**, 8760–8766.

59 T. G. Grissom, A. M. Plonka, C. H. Sharp, A. M. Ebrahim, Y. Tian, D. L. Collins-Wildman, A. L. Kaledin, H. J. Siegal, D. Troya, C. L. Hill, A. I. Frenkel, D. G. Musaev, W. O. Gordon, C. J. Karwacki, M. B. Mitchell and J. R. Morris, Metal-organic framework- and polyoxometalate-based sorbents for the uptake and destruction of chemical warfare agents, *ACS Appl. Mater. Interfaces*, 2020, **12**, 14641–14661.

60 J. S. Qin, D. Y. Du, W. Guan, X. J. Bo, Y. F. Li, L. P. Guo, Z. M. Su, Y. Y. Wang, Y. Q. Lan and H. C. Zhou, Ultrastable polymolybdate-based metal–organic frameworks as highly active electrocatalysts for hydrogen generation from water, *J. Am. Chem. Soc.*, 2015, **137**, 7169–7177.

